Molecular Crystals and Liquid Crystals

Publication details, including instructions for authors and subscription information:
http://www.tandfonline.com/loi/gmcl20

Ray-Tracing Simulations of Liquid-Crystal Devices

Maarten Sluijter [a], Dick K. G. de Boer [a] & H. Paul Urbach [b]

[a] Philips Research Europe, High Tech Campus, MS, AE Eindhoven, The Netherlands

[b] Optics Research Group, Department Imaging Science and Technology, Delft University of Technology, Lorentzweg, The Netherlands

Version of record first published: 01 Jun 2009

To cite this article: Maarten Sluijter, Dick K. G. de Boer & H. Paul Urbach (2009): Ray-Tracing Simulations of Liquid-Crystal Devices, Molecular Crystals and Liquid Crystals, 502:1, 164-177

To link to this article: http://dx.doi.org/10.1080/15421400902816983

Mol. Cryst. Liq. Cryst., Vol. 502, pp. 164–177, 2009

ISSN: 1542-1406 print/1563-5287 online
DOI: 10.1080/15421400902816983

Taylor & Francis
Taylor & Francis Group

Ray-Tracing Simulations of Liquid-Crystal Devices

Maarten Sluijter[1], Dick K. G. de Boer[1], and H. Paul Urbach[2]
[1]Philips Research Europe, High Tech Campus, AE Eindhoven, The Netherlands
[2]Optics Research Group, Department Imaging Science and Technology, Delft University of Technology, Lorentzweg, The Netherlands

In previous work, we have introduced the Hamiltonian method which enables to calculate the ray paths of light rays in inhomogeneous anisotropic media in the geometrical-optics approach. With this method we are able to simulate the effect of optical anisotropy in three dimensions. In this manuscript, we simulate the optical properties of multiple liquid-crystal configurations. We demonstrate the resemblance between the optical properties of a gradient-index fiber and a liquid-crystal layer with a Freédericksz alignment. In addition, we investigate the optical properties of artificial liquid-crystal profiles induced by the electric field of a set of point charges. Altogether, we conclude that, in the geometrical-optics approach, we are able to assess the optical properties of any arbitrary anisotropic optical system.

Keywords: geometrical optics; inhomogeneous anisotropic media; liquid crystal; optical anisotropy

1. INTRODUCTION

The problem of optical anisotropy in the geometrical-optics approach is classical and it is known for more than a century. However, most of the theory appears in a fragmented way and the propagation of waves through inhomogeneous anisotropic media is rarely addressed [1–10]. At the same time, the rapid advances in liquid-crystal applications, such as gradient-index lenses [11] or switchable lenticulars for auto-stereoscopic 2D/3D displays [12], call for a good exposition of the theory on wave propagation via inhomogeneous anisotropic media.

Address correspondence to Maarten Sluijter, Philips Research Europe, High Tech Campus 34, MS 31, AE Eindhoven 5656, The Netherlands. E-mail: Maarten.Sluijter@philips.com

In response to these developments, we have introduced a general ray-tracing method for inhomogeneous uniaxially anisotropic media [13]. In the manuscript presented below, we apply this general ray-tracing method in a numerical simulation program and demonstrate the optical properties of multiple liquid-crystal configurations.

One of the reasons that liquid crystal is so attractive, is that it can be controlled by external magnetic or electric fields. As a first example, we investigate the profile of a liquid-crystal layer applied between two parallel glass plates. This liquid-crystal profile can be controlled by an external electric field induced by a potential difference across the glass plates (for example, by means of conductive transparent ITO electrodes). The response of the liquid crystal to an external electric field is a threshold effect called the Freédericksz transition [14]. We will demonstrate that the optical properties of the liquid-crystal profile above the Freédericksz transition correspond to that of a gradient-index fiber. A gradient-index fiber is an optical fiber whose core has a refractive index that decreases with increasing radial distance from the fiber axis. Gradient-index fibers are designed in such a way, that light rays follow sinusoidal paths down the fiber. Similarly, we can show that light rays entering the liquid-crystal profile above the Freédericksz transition also follow similar ray paths. In addition to this result, the optical response of this liquid-crystal layer can be tuned by controlling the voltage that is applied across the glass plates.

Secondly, we investigate the liquid-crystal profile induced by the electric field due to multiple point charges placed inside a liquid crystal. Although the use of point charges is a rather artificial approach, it brings the idea of switchable gradient-index devices with more than two optical states to mind. Usually, liquid-crystal gradient-index devices are designed with a pattern of line electrodes that are able to change a liquid-crystal profile. We discuss a configuration of charges that are positioned at the grid points of a regular square grid. This concept of multiple electrodes introduces the possibility to increase the number of liquid-crystal configurations with only one optical system.

In what follows, we will present simulations of the optical properties of the two optical systems described above. In addition, we show that, in the geometrical-optics approach, we are able to assess the optical properties of complex inhomogeneous uniaxially anisotropic media in three dimensions.

2. LIQUID-CRYSTAL LIGHT GUIDE

As mentioned before, liquid crystal can be controlled by external magnetic or electric fields. Interactions between boundaries and liquid

crystal also have a large controlling effect. Often, the influence of the boundaries opposes the response to an external field. The result is a threshold phenomenon called the Freédericksz transition. In what follows, we will describe the Freédericksz transition of a liquid-crystal layer between two parallel glass plates.

2.1. Freédericksz Transition

We consider a simple geometry, defined by two parallel glass plates, separated by a distance h, as depicted in Figure 1. The space between the glass plates is filled with liquid crystal. The local optical axis inside a liquid crystal is called the director. The director $\hat{\mathbf{d}}$ aligns itself in the x-direction parallel to the glass surfaces. When an electric field $\mathbf{E}$ is applied in the z-direction, the liquid crystal deforms. The resulting deformation consists of both splay and bend deformations, but there is no twist deformation (cf. [14], p 32). Hence, the director $\hat{\mathbf{d}}$ lies in the xz-plane. For convenience, we can write the liquid-crystal profile in terms of an angle $\theta(z)$ which the director makes with the x-axis: $\hat{d}_x = \cos[\theta(z)]$, $\hat{d}_y = 0$ and $\hat{d}_z = \sin[\theta(z)]$. By minimizing the free energy, it can be deduced that $\theta(z)$ must satisfy the Euler equation (cf. [14], p 205). Then, the Euler equation, considering only the dominant terms, satisfies

$$K_{11}\frac{d^2\theta}{dz^2} + \varepsilon_0 \Delta\varepsilon E^2 \sin\theta\cos\theta = 0, \tag{1}$$

where E is the electric field strength and $\Delta\varepsilon = \varepsilon_{\|} - \varepsilon_{\perp}$ is the anisotropy in the dielectric permittivity of the liquid crystal. Note that the anisotropy mentioned here is not equivalent to the optical anisotropy. In addition, K_{11} is an elastic constant with which the associated splay deformation

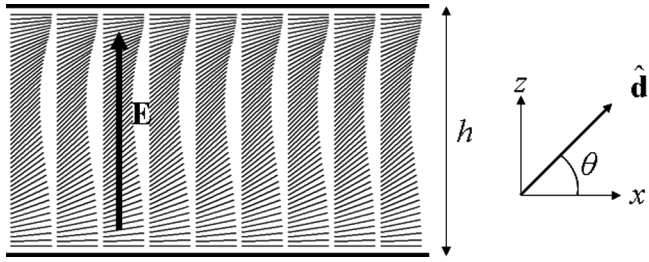

FIGURE 1 Director profile of liquid crystal in between two parallel glass plates, separated by a distance h. An electric field $\mathbf{E}$ is applied in the z-direction. As a result, the director $\hat{\mathbf{d}}$ is rotated by an angle θ towards the electric field direction. At $z = \frac{h}{2}$, the angle θ has a maximum value.

energies scale. Apparently, the distortion of the liquid crystal is dominated by splay deformation.

At this point, it is convenient to introduce the variable $\zeta = \frac{z}{h}$. From the symmetry of the system defined in Figure 1 we can deduce that $\frac{\partial\theta}{\partial\zeta} = 0$ at $\zeta = \frac{1}{2}$. As a result, we can define θ_{max} as the maximum value of θ at $\zeta = \frac{1}{2}$. Then, the potential difference across the liquid crystal layer that corresponds to θ_{max} can be written as (cf. [14], p 207)

$$V = 2\mathcal{K}(m)\sqrt{\frac{K_{11}}{\varepsilon_0 \Delta\varepsilon}}, \tag{2}$$

where $\mathcal{K}(m)$ is the complete elliptic integral of the first kind with elliptic modulus $m = \sin^2\theta_{max}$. In addition, there is a threshold voltage below which the liquid crystal remains undistorted, given by

$$V_{th} = \pi\sqrt{\frac{K_{11}}{\varepsilon_0 \Delta\varepsilon}}. \tag{3}$$

Above this threshold voltage, the director starts to rotate from its undistorted configuration towards the direction of the electric field. Note that the threshold voltage is independent of the distance h between the glass plates.

From Eq. (1), it can be shown that the angle $\theta(\zeta)$ can be written as (cf. [14], p 208)

$$\theta(\zeta) = \arcsin(\sin\phi \sin\theta_{max}), \tag{4}$$

where $\phi(\zeta)$ is the Jacobi amplitude of the incomplete elliptic integral of the first kind $F(\phi, m) = 2\mathcal{K}(m)\zeta$. Figure 2 shows $\theta(\zeta)$ for different voltages, expressed in terms of $V_r = \frac{V}{V_{th}}$. If $V_r = 1$, $\theta(\zeta) = 0^\circ$, whereas $\theta(\zeta) = 90^\circ$ if $V_r \to \infty$. The results are calculated for a sample with $K_{11} = 10^{-11}\,\mathrm{N}$ and $\Delta\varepsilon = 10$. These values are realistic estimates and yield a threshold voltage of 1.0558 V.

The director profile discussed in this section is called a Freédericksz alignment. In the next section, we will use the equations for the Freédericksz alignment to define the liquid-crystal profile between two parallel glass plates.

2.2. Simulations of a Liquid-Crystal Light Guide

In this section, we will simulate the optical properties of the liquid-crystal profile defined in Figure 1. The corresponding director profile is calculated analytically, using the formulas of the previous section.

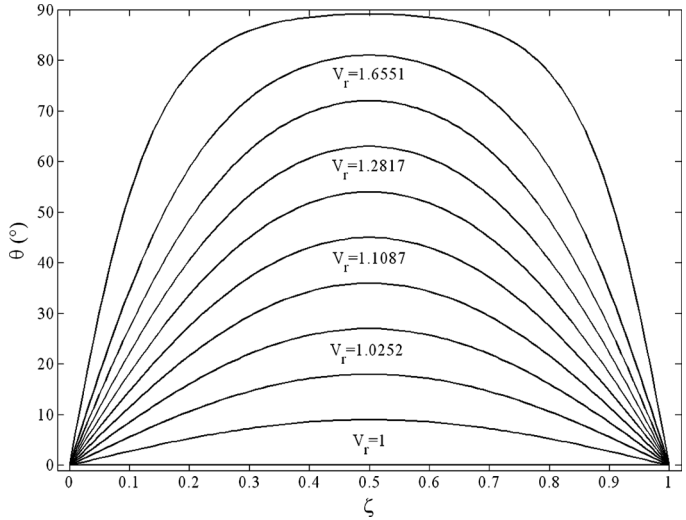

FIGURE 2 Distortion angle $\theta(\zeta)$ for several values of $V_r = \frac{V}{V_{th}}$. K_{11} is estimated 10^{-11} N and $\Delta\varepsilon$ is estimated 10 (at room temperature). In this case, the threshold voltage V_{th} is 1.0558 V.

In general, a light guide is an optical device which has the ability to 'guide' light. For example, optical fibers are light guides designed to guide light along its length. A gradient-index fiber is an optical fiber whose core has a refractive index that decreases with increasing radial distance from the fiber axis. Gradient-index fibers are designed in such a way, that light rays follow sinusoidal paths down the fiber, as depicted in Figure 3(a).

Figure 3(b) shows a liquid-crystal gradient-index device, whose optical properties are similar to those of the optical fiber in Figure 3(a). The difference is that the properties of the device in Figure 3(b) are inhomogeneous anisotropic. These anisotropic properties are defined by the director profile as depicted in Figure 1: the Freédericksz alignment extended in the x-direction. In contrast with the optical fiber in Figure 3(a), the anisotropic device in Figure 3(b) is not cylindrical: the liquid crystal layer has a thickness h.

We consider the liquid-crystal layer of Figure 3b. An incident light ray is linearly polarized in the xz-plane and propagates in the positive x-direction. At $(x,z) = \left(0, \frac{h}{2}\right)$ the light ray is injected into the liquid-crystal. For the calculation of the ray path inside the liquid crystal, we apply the Hamiltonian method for extraordinary rays (cf. [13], p 1269). With $\mathbf{r}$ the position and $\mathbf{p}_e$ the corresponding momentum

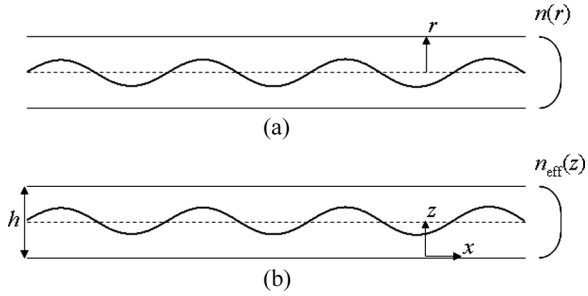

FIGURE 3 Gradient-index devices whose optical properties are (a) inhomogeneous isotropic and (b) inhomogeneous anisotropic. Figure (a) shows a gradient-index fiber whose index of refraction $n(r)$ depends on the radial distance r from the fiber axis. In Figure (b), the anisotropic properties are defined by the director profile as depicted in Figure 1. Then, the effective index of refraction $n_{\text{eff}}(z)$ depends on the vertical position z. These gradient-index devices are designed in such a way, that light rays follow sinusoidal paths down the fiber.

(i.e., the wave normal) of an extraordinary ray, the Hamilton equations are given by

$$\begin{aligned} \frac{d\mathbf{r}(\tau)}{d\tau} &= \nabla_p \mathcal{H}_e(\hat{\mathbf{d}}), \\ \frac{d\mathbf{p}_e(\tau)}{d\tau} &= -\nabla_r \mathcal{H}_e(\hat{\mathbf{d}}), \end{aligned} \tag{5}$$

where τ is a parameter which can be considered as time. In addition, the gradients $\nabla_p \mathcal{H}_e$ and $\nabla_r \mathcal{H}_e$ are defined

$$\begin{aligned} \frac{\partial \mathcal{H}_e}{\partial i} &= 2(n_e^2 - n_o^2)(\mathbf{p}_e \cdot \hat{\mathbf{d}}) \left(p_{ex} \frac{\partial \hat{d}_x}{\partial i} + p_{ey} \frac{\partial \hat{d}_y}{\partial i} + p_{ez} \frac{\partial \hat{dz}}{\partial i} \right), \\ \frac{\partial \mathcal{H}_e}{\partial p_{ei}} &= 2n_o^2 p_{ei} + 2(n_e^2 - n_o^2)(\mathbf{p}_e \cdot \hat{\mathbf{d}}) \hat{d}_i, \quad i = x, y, z \end{aligned} \tag{6}$$

where n_o and n_e are the ordinary and extraordinary index of refraction, respectively. These equations are a set of six coupled first-order differential equations for the vector components of the position $\mathbf{r}(\tau)$ and momentum $\mathbf{p}_e(\tau)$. By taking steps $\Delta\tau$ in the 'time' τ, the ray path $\mathbf{r}(\tau_0 + N\Delta\tau)$ and the corresponding momentum $\mathbf{p}(\tau_0 + N\Delta\tau)$, with $N \in \mathbb{N}$, are calculated by using the first-order Runge-Kutta method [15].

It is important to realize that the Hamiltonian method only applies when the properties of the medium change slowly with respect to the

wavelength. For the type of configurations we investigate, this condition is satisfied. Hence, the use of the Hamiltonian method is justified.

We simulate a nematic liquid crystal with $n_o = 1.5266$ and $n_e = 1.8181$ (BL009 mixture [16]). We define $K_{11} = 10^{-11}\,\mathrm{N}$ and $\Delta\varepsilon = 10$, yielding a threshold voltage of 1.0558 V. The ray paths are calculated with step size $\Delta\tau = 0.001$ and $h = 5$. Note that h is a dimensionless number that can be scaled to any desired dimension, as long as the properties of the medium change slowly with respect to the wavelength of light. Figure 4 shows the results for six extraordinary ray paths. Each individual ray path is calculated in a different Freédericksz alignment. Each alignment corresponds to a value for $V_r = \frac{V}{V_{th}} = \frac{2}{\pi}\mathcal{K}(m)$, where the elliptic modulus $m = \sin^2\theta_{max}$. The maximum value of V_r is 1.1803, corresponding to a voltage $V = 1.2461\,\mathrm{V}$ and $\theta_{max} = \frac{\pi}{4}$ radians.

The angle at which the light is refracted at the position $(x,z) = \left(0,\frac{h}{2}\right)$ increases since the angle θ_{max} increases with the voltage. As a result, we can expect that the period of the sinusoid decreases with increasing voltage. Figure 4 shows that this expectation is confirmed by the simulations. In addition, from Figure 4, we can conclude that the ray paths are sinusoidal.

We have analyzed the behavior of light rays inside liquid crystal with a Freédericksz alignment. From the results, we can conclude that

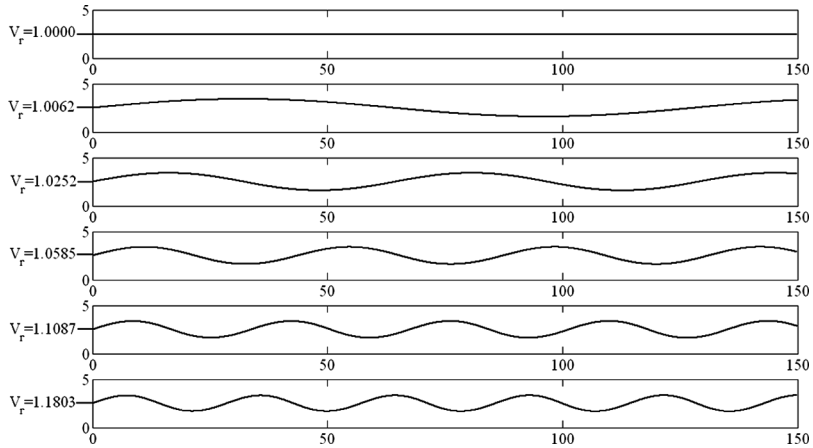

FIGURE 4 Ray paths of extraordinary rays for different Freédericksz alignments ($K_{11} = 10^{-11}\,\mathrm{N}$, $\Delta\varepsilon = 10$). The incident rays are in the horizontal direction and are refracted by the liquid crystal layer at $(x,z) = \left(0,\frac{h}{2}\right)$. The liquid crystal has refractive indices $n_o = 1.5266$ and $n_e = 1.8181$. The period of the sinusoids decreases with increasing voltage.

the optical behavior of the studied liquid-crystal layer is similar to the optical behavior of a gradient-index fiber: the liquid crystal can act as a light guide. In addition, the optical response of the liquid-crystal layer can be tuned by controlling the voltage that is applied across the glass plates.

3. ARTIFICIAL LIQUID-CRYSTAL SPATIAL LIGHT MODULATOR

In this section, we apply the Hamiltonian method to light rays entering a three-dimensional inhomogeneous liquid crystal. In this case, the director profile of the liquid crystal is induced by the electric field of one or more point charges. Obviously, the use of point charges is a rather artificial approach. However, in this section, we aim to investigate the idea of small electrodes for controlling the director profile of a liquid crystal. First, we investigate the optical behavior of one point charge inside a liquid crystal. Then, we investigate the optical properties of a configuration of multiple point charges inside a liquid crystal.

3.1. Single Point Charge in a Liquid Crystal

Below, we briefly discuss the results of ray-tracing simulations for a single point charge in a liquid crystal as presented in [13]. We consider a Cartesian coordinate system in which the plane $z = 0$ is defined as a grounded conducting plate with electric potential $\Phi = 0$. Let there be a point charge in $(0, 0, a)$, for some $a > 0$, with positive charge q, see Figure 5. Using the method of images [17], we can write the electric potential due to the charge q for $z \geq 0$ as

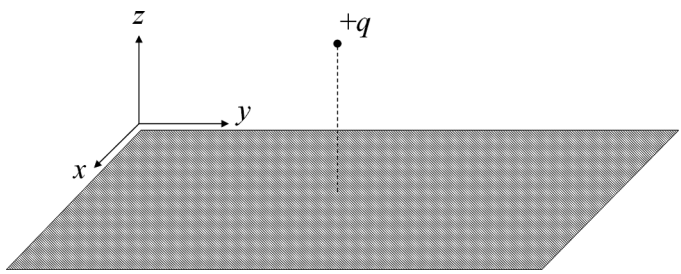

FIGURE 5 Point charge q at a distance a above the origin. The plane $z = 0$ is defined a grounded conducting plate. As a result, there is an electric field in the half-space $z \geq 0$.

$$\Phi(x,y,z) = \frac{q}{4\pi\varepsilon_0}\frac{1}{\sqrt{x^2+y^2+(z-a)^2}} - \frac{q}{4\pi\varepsilon_0}\frac{1}{\sqrt{x^2+y^2+(z+a)^2}}. \quad (7)$$

The corresponding electric field is then given by $\mathbf{E}(x,y,z) = -\nabla\Phi(x,y,z)$. Let the space $z \geq 0$ be filled with a nematic liquid crystal. We will assume that the field is so high, that all directors follow the field direction. This means that the electric energy is considered to be much higher than the elastic energy between the directors. Hence, the director profile due to the electric field of the point charge q is:

$$\hat{\mathbf{d}}(x,y,z) = \frac{E(x,y,z)}{|E(x,y,z)|}, \quad z \geq 0. \quad (8)$$

Figure 6 shows the director profile in the xz-plane for $a = 50$, $x \in [-50, 50]$ and $z \in [0, 100]$. The liquid crystal in the upper half-space $z \geq 0$ has an ordinary index of refraction $n_o = 1.5$ and an extraordinary index of refraction $n = 1.7$. The lower half-space $z < 0$ is assumed to be glass with an index of refraction $n_{\text{glass}} = 1.5$.

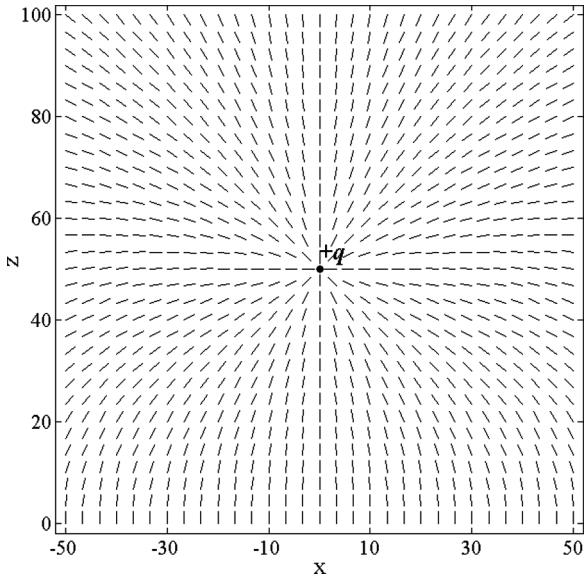

FIGURE 6 The director profile (i.e., the normalized electric field due to the point charge q) in the xz-plane for $a = 50$, $x \in [-50, 50]$ and $z \in [0, 100]$. The profile has azimuthal symmetry.

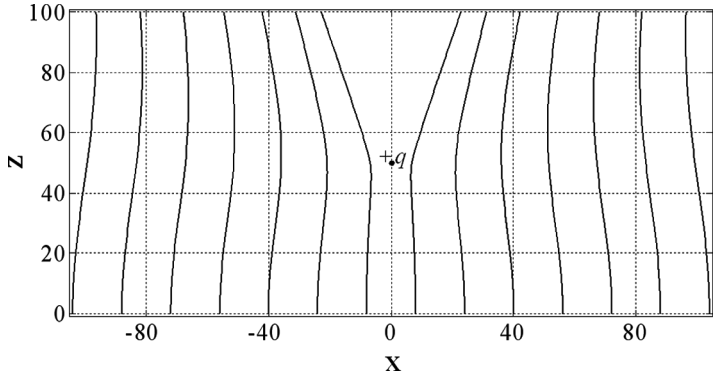

FIGURE 7 Ray paths of several extraordinary waves at normal incidence to the plane $z = 0$, where the xz-plane is the plane of incidence. Note the 'curtain-like' behavior, allowing no light in the region above the point charge.

We will use the Hamilton equations to calculate the ray paths of waves that are injected into the liquid crystal. Inside the liquid crystal, we calculate the ray paths of extraordinary waves by using Eqs. (5) and (6). By taking small steps in the parameter τ, the position $\mathbf{r}(\tau)$ and momentum $\mathbf{p}_e(\tau)$ are calculated using the first-order Runge-Kutta method.

Figure 7 shows several ray paths of extraordinary waves at normal incidence to the plane $z = 0$. The plane of incidence is the xz-plane. Apparently, light is absent in the region above the point charge q and the ray paths seem to form a 'curtain-like' appearance.

At $z = 100$, a matrix of intervals in x and y is defined which is used to collect the x- and y-coordinates of ray paths. The number of rays collected by each interval is a measure for the intensity. Then, the spatial intensity distribution at $z = 100$ should give us an idea of the optical behavior.

We define rays of light propagating in the z-direction incident on the (transparent) conducting plate. The initial positions of the rays (x_0, y_0, z_0) randomly lie inside a square defined by $x_0 \in [-10, 10]$ and $y_0 \in [-10, 10]$. These rays are refracted at the conducting plate at $z = 0$, where $\hat{\mathbf{d}} = (0, 0, -1)$. We perturb the incident angle of the rays to 10^{-6} degrees in the xz-plane. In addition, we define a linear polarization parallel to the xz-plane. As a result, the refracted waves are extraordinary waves and therefore Eqs. (5) and (6) can be applied.

Figure 8 shows the intensity distribution I at $z = 100$. The number of rays that is traced is 30000. The white square indicates the boundary in which the initial positions (at $z = 0$) of the incident rays lie.

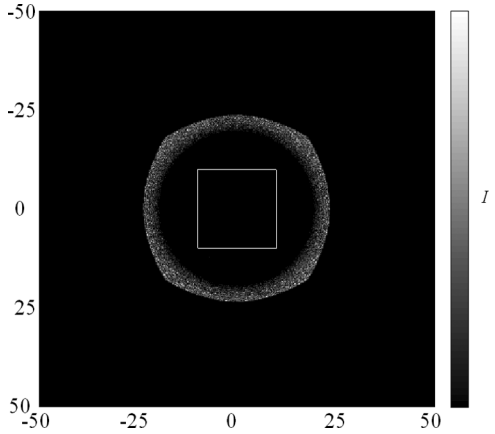

FIGURE 8 Intensity distribution I at $z = 100$ for $x \in [-50, 50]$ and $y \in [-50, 50]$. The square (white) indicates the boundary in which the initial positions of the incident rays lie.

The center of the square is exactly below the point charge. Apparently, the square light source at $z = 0$ is transformed into a circular like light distribution at $z = 100$.

3.2. Multiple Point Charges in a Liquid Crystal

In the previous section, we have analyzed the optical properties of a single point charge inside a nematic liquid crystal. In this section, we investigate the optical properties of the same optical system, but now with a configuration of 9 point charges inside a nematic liquid crystal. The positions of the 9 point charges in the xy-plane at $z = 50$ is defined as depicted in Figure 9. The distance between the individual point charges is indicated by u. In addition, the middle point charge is positioned exactly above the origin ($x = y = 0$). In Figure 9(a), all the point charges are positively charged whereas in Figure 9(b), one point charge is negatively charged.

Similar to the approach used in the previous section, we use the method of images to calculate the electric field $\mathbf{E}(x, y, z)$ for $z \geq 0$ and the resulting director profile $\hat{\mathbf{d}}$ (see Eq. (8)). In addition, we apply the Hamilton equations to calculate the ray paths of extraordinary rays in a liquid crystal with indices of refraction $n_o = 1.5$ and $n_e = 1.7$. The initial positions of the rays (x_0, y_0, z_0), propagating in the positive z-direction, randomly lie inside a square defined by $x_0 \in [-10, 10]$ and $y_0 \in [-10, 10]$. The rays are refracted at the liquid-crystal interface

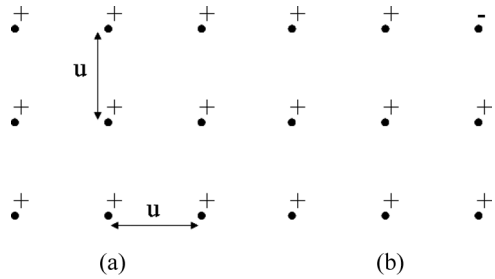

FIGURE 9 Positions of the point charges in the xy-plane at $z = 50$. The distance between the individual point charges is indicated by u. In Figure (a) all the point charges are positively charged whereas in Figure (b) one point charge is negatively charged.

and modulated by the liquid crystal in the half space $z \geq 0$. At $z = 100$, we calculate the spatial intensity distribution I.

Figure 10 shows the intensity distribution I at $z = 100$ for the configuration depicted in Figure 9(a). In this case, $u = \frac{20}{3}$. The number of rays that is traced is 150000. The white square indicates the boundary in which the initial positions (at $z = 0$) of the incident rays lie. The center of the square is exactly at the origin. As can be seen from Figure 7, the light rays are repelled in the neighborhood of a point charge. Hence, we can expect that light rays will converge in the regions

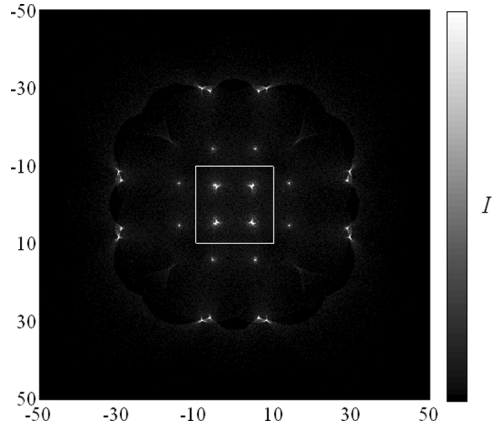

FIGURE 10 Intensity distribution I for the configuration of Figure 9(a) at $z = 100$ for $x \in [-50, 50]$ and $y \in [-50, 50]$ and $u = \frac{20}{3}$. The square light source at $z = 0$ (indicated by the white square) is transformed to a configuration of light spots that lie on the grid points of a regular square grid.

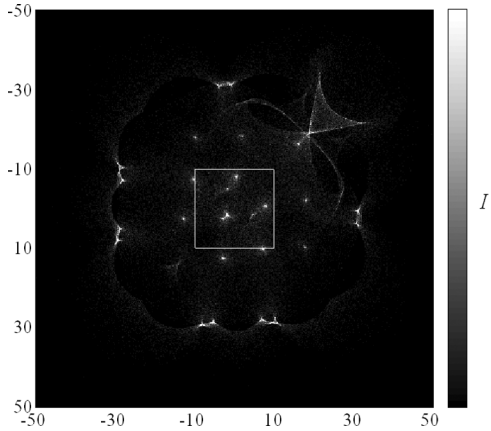

FIGURE 11 Intensity distribution I for the configuration of Figure 9(b) at $z = 100$ for $x \in [-50, 50]$ and $y \in [-50, 50]$ and $u = \frac{20}{3}$. Although we define a different charge distribution of the point charges, we apply the same optical system used in Figure 10. In this case, the intensity distribution I at $z = 100$ shows both light spots and blurring effects.

between multiple point charges with the same charge. Indeed in Figure 10, we clearly see that the square light source at $z = 0$ is transformed into multiple light spots at $z = 100$. Moreover, this collection of light spots lies on the grid points of a regular square grid, similar (but not identical) to the configuration of point charges.

Figure 11 shows the intensity distribution I at $z = 100$ for the configuration depicted in Figure 9(b). This configuration of point charges corresponds to the same optical system, but with a different charge sign distribution. Similar to the intensity distribution I in Figure 10, the eight positive point charges converge the light rays to light spots at $z = 100$. On the other hand, the negatively charged point charge on the right side is responsible for a different optical response. Clearly, the combination of positive and negative point charges is responsible for a diverging effect. As a result, the square light source at $z = 0$ is transformed to a spatial light distribution which shows both light spots and blurring effects.

From the results of this section, we can conclude that charges positioned on the grid points of a regular square grid in a liquid crystal can produce multiple spatial light distributions. The optical response of the optical system can be changed by controlling the amount of positive and negative charge. From these considerations, the optical system discussed can be interpreted as a switchable liquid-crystal spatial light modulator.

4. CONCLUSIONS

From the simulations presented in this manuscript we can conclude that, in the geometrical-optics approach, we are able to assess the optical properties of arbitrary inhomogeneous uniaxially anisotropic media in three dimensions. The Hamiltonian method and the corresponding Hamilton equations form an appropriate tool to analyze the optical properties of uniaxially anisotropic optical systems. In two examples, we have investigated the optical properties of a liquid-crystal configuration. For both configurations, we can conclude that the analysis has produced plausible results. Moreover, it has been shown that the proposed liquid-crystal configurations show the characteristics of a light guide and a spatial light modulator.

REFERENCES

[1] Stavroudis, O. N. (1962). *J. Opt. Soc. Am.*, *52*, 187.
[2] Swindell, W. (1975). *Appl. Opt.*, *14*, 2298.
[3] Simon, M. C. & Echarri, R. M. (1986). *Appl. Opt.*, *25*, 1935.
[4] Trolinger, J. D., Chipman, R. A., & Wilson, D. K. (1991). *Opt. Eng.*, *30*, 461.
[5] McClain, S. C., Hillman, L. W., & Chipman, R. A. (1993). *J. Opt. Soc. Am. A*, *10*, 2371.
[6] McClain, S. C., Hillman, L. W., & Chipman, R. A. (1993). *J. Opt. Soc. Am. A*, *10*, 2383.
[7] Avendaño-Alejo, M. & Stavroudis, O. N. (2002). *J. Opt. Soc. Am. A*, *19*, 1674.
[8] Panasyuk, G., Kelly, J. R., Gartland, E. C., & Allender, D. W. (2003). *Phys. Rev. E*, *67*, 041702.
[9] Panasyuk, G., Kelly, J. R., Bos, P., Gartland, E. C., & Allender, D. W. (2004). *Liquid Crystals*, *31*, 1503.
[10] Jenkins, C. *et al*., (2007). *J. Opt. Soc. Am. A*, *24*, 2089.
[11] Kraan, T. C., van Bommel, T., & Hikmet, R. A. M. (2007). *J. Opt. Soc. Am. A*, *24*, 3467.
[12] Sluijter, M., IJzerman, W. L., de Boer, D. K. G., & de Zwart, S. T. (2006). *Proc. SPIE*, *6196*, 61960I.
[13] Sluijter, M., de Boer, D. K. G., & Braat, J. J. M. (2008). *J. Opt. Soc. Am. A*, *25*, 1260.
[14] Collings, P. J. & Hird, M. (1997). *Introduction to Liquid Crystals, Chemistry and Physics*, Taylor & Francis: London, UK.
[15] Press, W. *et al*., (1992). *Numerical Recipes in FORTRAN, The Art of Scientific Computing*, Cambridge University Press: Cambridge, UK.
[16] EMD Chemicals Inc., Polymer Dispersed Liquid Crystals, http://www.emdpigments.com/optics/PDLC%20brochure.pdf
[17] Jackson, J. D. (1999). *Classical Electrodynamics*, John Wiley & Sons: New York, US.